The Astrophysical Journal, 581:1180–1193, 2002 December 20

H_2O MASERS AND SUPERSONIC TURBULENCE

V. Strelnitski,[1,2] J. Alexander,[2,3] S. Gezari,[1,4,5] B. P. Holder,[1,6,7] J. M. Moran,[8] and M. J. Reid[8]
Received 1998 November 12; accepted 2002 August 19

ABSTRACT

We use unpublished and published VLBI results to investigate the geometry and the statistical properties of the velocity field traced by H_2O masers in five galactic regions of star formation: Sgr B2(M), W49N, W51(MAIN), W51N, and W3(OH). In all sources the angular distribution of the H_2O hot spots demonstrates approximate self-similarity (fractality) over almost 4 orders of magnitude in scale, with the calculated fractal dimension d between $\approx$0.2 and 1.0. In all sources, the lower order structure functions for the line-of-sight component of the velocity field are satisfactorily approximated by power laws, with the exponents near their classic Kolmogorov values for high Reynolds number incompressible turbulence. These two facts, as well as the observed significant excess of large deviations of the two-point velocity increments from their mean values, strongly suggest that the H_2O masers in regions of star formation trace turbulence. We propose a new conceptual model of these masers in which maser hot spots originate at the sites of ultimate dissipation of highly supersonic turbulence produced in the ambient gas by the intensive gas outflow from a newly born star. Because of the high brightness and small angular sizes of masing hot spots and the possibility of measuring their positions and velocities with high precision, they become a unique probe of supersonic turbulence.

Subject headings: ISM: jets and outflows — masers — turbulence

1. INTRODUCTION

The idea of an energy cascade through a hierarchy of scales (Richardson 1922; Kolmogorov 1941a; Obukhov 1941), the phenomenological theory of turbulent energy dissipation (Kolmogorov 1941b, 1941c), and the experimental and theoretical results related to the intermittency of turbulent velocity fields (see Frisch 1995 for references) are the cornerstones of the present understanding of incompressible turbulence. Much less is known about compressible (supersonic) turbulence. Analytical approaches and laboratory experiments are still limited to low Mach numbers, $M \approx 1$, and the results of numerical simulations may depend crucially on the adopted boundary and initial conditions.

Von Weizsäcker (1951) was the first to point out that the interstellar medium (ISM) is characterized by very high Reynolds numbers and high Mach numbers, and thus highly supersonic turbulence should be its typical state. Much work using the ISM to study supersonic turbulence has since been attempted (see, e.g., Dickman 1985; Scalo 1987; Falgarone & Phillips 1990; Elmegreen 1993; Franco & Carraminana 1999). However, at the relatively large scales considered so far, 10^{21}–10^{17} cm, the ISM may not be an adequate laboratory for studying supersonic turbulence in the traditional sense of the term "turbulence." The initially hypothesized turbulent energy cascade from the largest to the smallest scales of the ISM, initiated by the differential rotation of the Galaxy (von Weizsäcker 1951; Fleck 1981), is an obvious idealization. Even if the differential rotation works as the major energy source for the observed turbulence in the neutral gas at the periphery of galaxies (Sellwood & Balbus 1999), it should be disrupted by the powerful injection of energy from supernovae and stellar winds at intermediate scales in the major galactic disk (Spitzer 1978). ISM turbulence at large and intermediate scales is also complicated by the effects of self-gravitation.

It has recently been recognized that the 1.35 cm wavelength H_2O masers (see reviews on masers in Elitzur 1992; Clegg & Nedoluha 1993; Migenes & Reid 2002) may be promising tools for the study of "Kolmogorov-type" supersonic turbulence. VLBI studies of the proper motions of several bright H_2O maser sources associated with newly born stars have revealed expansion of the clusters of maser spots, participating in gas outflows from these stars (see Anderson & Genzel 1993 for a review). This type of regular motion had been theoretically predicted before its discovery (Strelnitski & Sunyaev 1973). In some cases, including W49N, there are also indications of another regular component in the velocity field revealed by the masers: rotation (Reid et al. 1988; Gwinn, Moran, & Reid 1992). However, besides these regular components, VLBI measurements indicated the presence of a residual *random* component of motion. Typically, approximating the proper motion vectors by a simple model of expanding and rotating gas leaves a residual dispersion of $\approx$15 km s^{-1} per axis, which is considerably larger than the errors of these observations (Reid et al. 1988). This value corresponds to $\approx\sqrt{3} \times 15 \approx 26$ km s^{-1} for the total velocity vector and can be considered the characteristic turbulent velocity dispersion at the largest spatial scale covered by the maser cluster.

Walker (1984), using the VLBI maps of the H_2O source in W49N obtained by Walker, Matsakis, & Garcia-Barreto (1982), demonstrated that both the two-point velocity increments and the two-point spatial correlation function show power-law dependencies on maser spot separation. This

[1] Maria Mitchell Observatory, 3 Vestal Street, Nantucket, MA 02554.
[2] New Mexico Institute of Mining and Technology, Department of Physics.
[3] Current address: Luxel Corporation, Friday Harbor, WA 98250.
[4] Brown University.
[5] Current address: Department of Astronomy, Columbia University, New York, NY 10027.
[6] Wesleyan University.
[7] Current address: Department of Physics, University of Texas at Austin, Austin, TX 78712.
[8] Harvard-Smithsonian Center for Astrophysics, 60 Garden Street, Cambridge, MA 02138.

behavior is typical of a turbulent flow, although Walker did not favor the turbulence interpretation. Gwinn (1994) carried out a similar statistical analysis using better VLBI results for W49N obtained by Gwinn et al. (1992). He confirmed the power-law dependency of velocity dispersion and spatial density of masing spots on spatial scale and ascribed this behavior to turbulence.

This paper summarizes a series of our studies of H_2O masers as tracers of supersonic turbulence in regions of star formation. Preliminary results were reported by Strelnintski et al. (1998), Holder & Strelnitski (1997), Gezari (1997), and Gezari, Reid, & Strelnitski (1998). In § 2 we present our VLBI results for the H_2O maser source in Sgr B2(M). The geometrical properties of supersonic turbulence revealed by H_2O masers in this and four other sources are presented in § 3, and the statistical properties of the velocity field traced by the masers are given in § 4. In § 5, proceeding from the hypothesis that the H_2O masers adequately probe the velocity field of turbulence, we discuss implications of our statistical results for the theory of supersonic turbulence. In § 6 we describe a new conceptual model of H_2O masers in regions of star formation based on the surmised connection of maser pumping with the sites of ultimate dissipation of turbulent energy. Conclusions are summarized in § 7.

2. VLBI OBSERVATIONS OF Sgr B2(M)

The observations of Sgr B2(M) were conducted on 1986 January 23, February 26, March 27, and April 26 as part of a campaign to measure proper motions of these H_2O masers. Four telescopes spanning the US were used: the Haystack 37 m telescope in Westford, Massachusetts; the National Radio Astronomy Observatory[9] (NRAO) 43 m telescope in Green Bank, West Virginia; one 25 m telescope of the Very Large Array (VLA) near Socorro, New Mexico; and the Owens Valley Radio Observatory (OVRO) 40 m telescope in Big Pine, California. The Mk III recording system was used with four 2 MHz bands covering the LSR velocity ranges of -40 to -14, 18–43, 43–69, and 68–94 km s^{-1}, assuming a rest frequency of 22235.08 MHz for the H_2O 6_{16}–5_{23} transition. The recorded data were correlated at the Mk III processor at Haystack Observatory in a mode that yielded 56 (uniformly weighted) spectral channels, each 35.71 kHz or 0.48 km s^{-1} wide.

The data were edited, calibrated, and imaged following the same general procedures as described in Reid et al. (1988) for the source Sgr B2(N). The synthesized interferometer beam was approximately 2.4×0.4 mas FWHM, elongated in the north-south direction, owing to the low declination of Sgr B2. Compact maser spots with flux densities ranging between 135 and 0.4 Jy were detected across a field of approximately $2'' \times 2''$. The positions of the maser spots were obtained by fitting a circular Gaussian brightness model for each spectral channel independently using the AIPS task IMFIT.

3. THE GEOMETRY OF H_2O MASERS

Figure 1 shows a series of decreasing spatial scales for our VLBI map of Sgr B2(M). The scale changes by almost 4 orders of magnitude (from $\gtrsim 1''$ down to $\lesssim 1$ mas), which, at the assumed distance of 8 kpc (Reid 1993), corresponds to a range of linear scales between, roughly, 10,000 and 1 AU. As is typical of fractal dust–like structures, the distribution of masers looks qualitatively the same on all scales, with evident clustering.

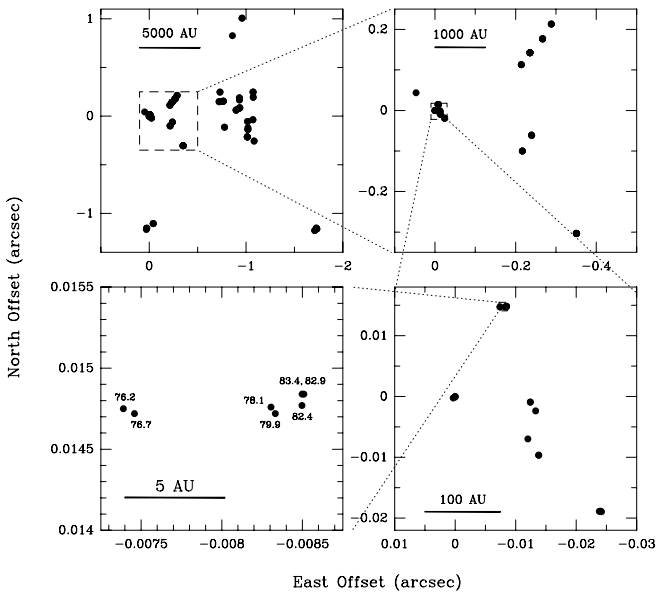

FIG. 1.—Multiscale VLBI maps of H_2O maser source in Sgr B2(M) as observed on 1986 January 23. On all maps except the last one, dot sizes are larger than maser spot sizes. On the last map, dots are smaller than observed maser spot sizes ($\sim$1 AU, which is perhaps affected by interstellar scattering). The dots on the last map show measured positions of spectral channels whose radial velocities are indicated near the dots.

On all maps of Figure 1, except the last one, dot sizes are larger than the typical observed size of an individual maser spot. Dots on the last map show measured positions of spectral channels. Since a spectral channel (0.48 km s^{-1}) is narrower than a typical spectral width of a single spot ($\gtrsim 0.8$ km s^{-1}), a dot on the last map typically represents the position and velocity of only a part of an individual spot. We call the smallest groupings of heavily blended individual spots "minimal clusters." The dots on the map only approximate the extension of and the velocity dispersion in these minimal clusters. Inspection of the available data indicates that a typical size of a minimal cluster is a few AU. The velocity dispersion within minimal clusters varies from ≈ 1 to 5 km s^{-1}.

We used two methods to estimate the fractal dimension of the spatial distribution of H_2O masers in Sgr B2(M): the "density-radius" and the "box-counting" methods (see, e.g., Crownover 1995; Feder 1988). The density-radius measure is based on the generalization of the mass versus radius relation for objects of integer dimension,

$$M \propto r^d \,, \tag{1}$$

where d is the dimension of the object. Equation (1) can be used as a general definition of the dimension of an object, including objects whose average density changes in a self-similar way with changing scale (e.g., Mandelbrot 1982). For these objects (fractals) d is noninteger. Average density ρ within a given volume V is M/V. Therefore,

$$\rho = \frac{M}{V} \propto \frac{r^d}{r^{d_0}} = r^{d-d_0} \,, \tag{2}$$

[9] NRAO is a facility of the National Science Foundation, operated under cooperative agreement by the Associated Universities, Inc.

where d_0 is the dimension of the supporting space, e.g., $d_0 = 2$ for a plane. If the dimension of the object equals the dimension of the support, ρ equals a constant. If not, ρ is a function of r. The steepness of this function depends on d.

A more practical procedure results from differentiating equation (1), which gives

$$\sigma \equiv \frac{dM}{dV} \propto r^{d-d_0} , \tag{3}$$

or

$$d = \frac{d(\log \sigma)}{d(\log r)} + d_0 . \tag{4}$$

Determining the dimension is thus reduced to measuring the slope of $\log \sigma$ versus $\log r$. In the case of a point set like ours, "density" means "number density."

In our numerical procedure, σ is calculated (for a discrete set of r-values) as the surface density of companions to a given maser hot spot at angular separation r, averaged over all maser spots:

$$\sigma(r) = \frac{\langle \text{number of points}(r, r + \delta r) \rangle}{\pi[2r\delta r + (\delta r)^2]} . \tag{5}$$

The same procedure was used by Walker (1984) and Gwinn (1994) for demonstrating self-similar clustering of H_2O masers in W49N. However, these authors did not relate $\sigma(r)$ to the fractal dimension of the source. Larson (1995) uses a similar procedure to obtain a fractal dimension for a young stellar association in Taurus.

We tested our numerical procedure by obtaining the density-radius fractal measure of a simple straight line and of the classical mathematical fractal, a Sierpinski triangle. The measured dimensions of 1.00 and 1.58 were in excellent agreement with their theoretical values $d = 1.000$ and ≈ 1.585, respectively.

The box-counting measure associates a fractal object's dimension d with the number N of boxes of side length l needed to cover the object (Crownover 1995):

$$N(l) \propto l^{-d} . \tag{6}$$

The graph of $\log N(l)$ versus $\log l$ is a straight line, having slope $-d$. We used the following computational algorithm. The square plane of minimal side length L containing the whole object is divided into 2^2 equal squares of side length $L/2$. The number of these squares containing one or more points making up the object is determined and stored. Each nonempty square of side length $L/2$ is subdivided again into four squares of equal area; the number of nonempty squares of side length $L/4$ is determined and stored, etc. The procedure is repeated down to some minimal side length of subsquares; minimal side length is determined by the characteristic length of the smallest features of the object. The logarithm of the number of nonempty squares versus logarithm of their side length is plotted, and the slope of the straight line fitting the data points is measured; this slope is equal to $-d$. This numerical procedure was also tested with a straight line and a Sierpinski triangle. The measured values of dimension were again in agreement with the theoretical values.

We used equation (4) to determine the fractal dimension of the two-dimensional projected ($d_0 = 2$) H_2O masers in the four observations of Sgr B2(M). The values of the fractal dimension for the four observations and for their average are indicated in the corresponding panels of Figure 2. The average value is $d_2 \approx 0.44 \pm 0.07$. The box-counting result for the average of the four observations is shown in Figure 3. The ensuing fractal dimension, $d_2 \approx 0.21 \pm 0.02$, is noticeably lower than that obtained from the density-radius plot.

For both measures, a single linear fit is a satisfactory first approximation; the standard deviation of the residuals to

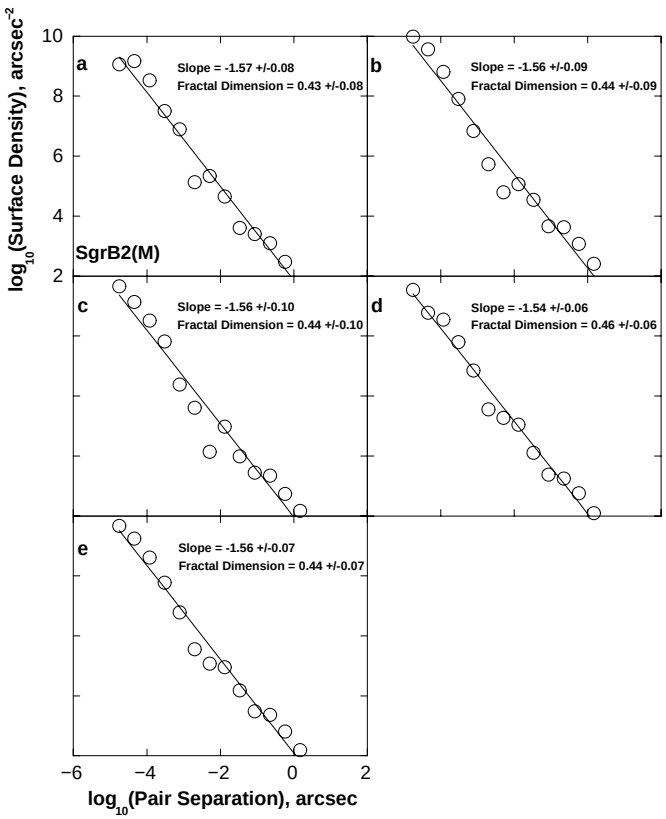

FIG. 2.—Density-radius fractal measure for H_2O maser source in Sgr B2(M) for (*a*)–(*d*) the four epochs of observation and (*e*) their average. The solid straight line shows a linear fit to the data points (*open circles*).

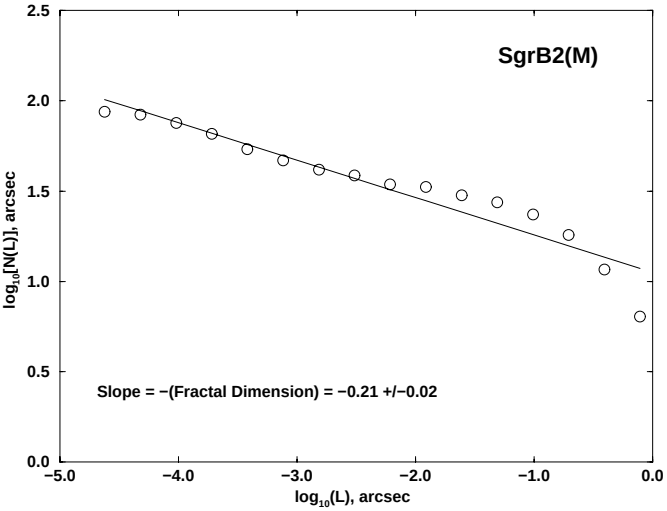

FIG. 3.—Box-counting fractal measure for H_2O maser source in Sgr B2(M); average for the four epochs of observation.

the fit does not surpass $\pm 10\%$ for each epoch of observations and for the combined fit. However, notable deviations from a single power-law approximation can be seen in Figures 2 and 3. For example, a higher fractal dimension for the largest scales is evidenced by the steeping slope of the points in Figure 3. Some deviation from the linear dependence is seen in Figure 2, between log(separation) ≈ -2 and -3. It may indicate some depression of clustering at the scales around $0\farcs003$ ($\sim 10^{14}$ cm for this source).

The origin of the systematic difference between the two applied fractal measures is unclear. It may be rooted in technical particularities of the methods. Some practical problems in the application of the box-counting method are discussed in Gouyet (1996, § 1.4.4). This discussion indicates that derived fractal dimensions should be correct within a factor of 2. Given this uncertainty and the range of the derived values of slopes in Figures 2 and 3, we estimate the fractal dimension of the observed cluster as $d_2 \approx 0.3 \pm 0.2$.

Gwinn (1994) performed a statistical analysis of the VLBI maps of W49/H_2O obtained by Gwinn et al. (1992). He demonstrated a power-law dependence of the number density of neighbors on their separation. However, he used the one-dimensional projection of the distance and did not interpret his results in terms of fractals. To make results for W49N comparable to those for Sgr B2(M), we applied the density-radius fractal measure to the two-dimensional spatial distribution of the H_2O maser spots in W49N, using the VLBI positions published by Gwinn et al. (1992). We have applied this measure to three more sources: two with published VLBI results, W51(MAIN) and W51N (Genzel et al. 1981; Schneps et al. 1981), and one source, W3(OH), for which we used our unpublished VLBI coordinates of the maser spots (the corresponding map of the source was published; Alcolea et al. 1992).

The results for all sources are shown in Figure 4. A power-law dependence is a good approximation for all of them, and it gives a low fractal dimension, $\lesssim 1$, for all the observed sets of maser spots as projected on the sky.

Given the small angular dimensions of maser clusters ($\sim 1''$), their projection on the sky is essentially an orthogonal projection. Therefore, the dimension d_3 of the real fractal, residing in three-dimensional space, coincides with the dimension, d_2, of its two-dimensional projection if $d_3 = d_2 < 2$ (e.g., Falconer 1990). We have demonstrated above that this condition is fulfilled for H_2O masers. Thus, we conclude that the fractal dimension of H_2O clusters in all five of the sources we have studied is low, $d_3 \lesssim 1$.

This conclusion is new, although Walker (1984) and Gwinn (1994) obtained results that can be converted to estimates of fractal dimension. Walker (1984) obtained a high negative value of the power index (approximately -1.1) in the power-law approximation of the density-radius dependence for W49N/H_2O. This corresponds to a fractal dimension $d_3 = d_2 \approx 0.9$. Gwinn (1994) reduced his two-point correlation analysis of H_2O masers in W49N to the one-dimensional projection of the observed map on the x-axis.

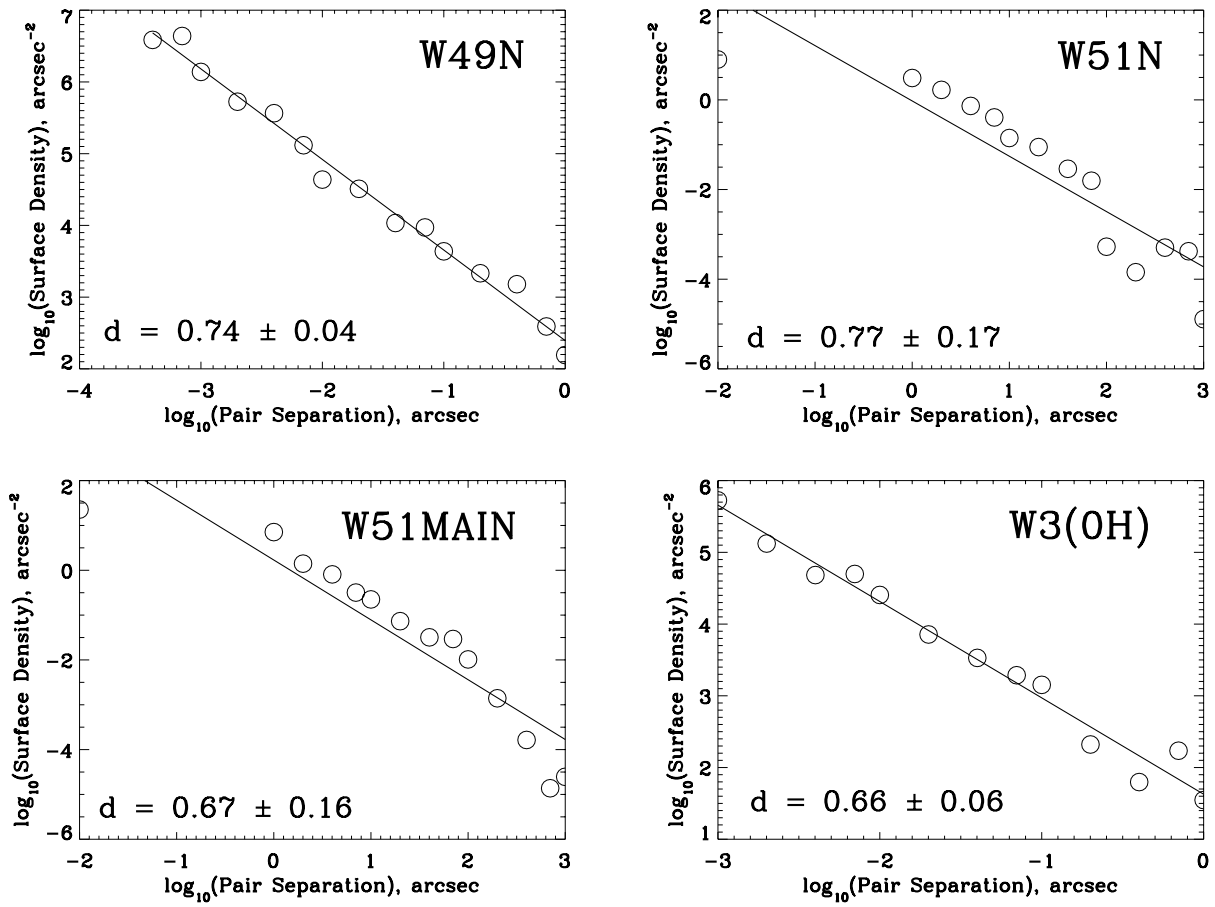

FIG. 4.—Density-radius fractal measure for the H_2O maser sources in W49N, W51(MAIN), W51N, and W3(OH). [*Note in proof*.—The x-axis unit for W51MAIN and W51N is milliarcsec, not acrsec.]

He obtained a power index, $\gamma_1 \approx -(0.2\text{–}0.3)$, for a large interval of scales. Although he did not connect this result with a fractal dimension, we note that for a one-dimensional projected fractal, $d_1 = \gamma_1 + 1$, where d_1 is the fractal dimension of the one-dimensional projection of the real fractal residing in three-dimensional space. Thus, Gwinn's result corresponds to $d_1 \approx 0.7\text{–}0.8$. Since $d_1 < 1$, the same fractal dimension is ascribed to both the two-dimensional projection and the real fractal residing in three-dimensional space. Thus, both the Walker (1984) and Gwinn (1994) results support our conclusion that the fractal dimension of H_2O clusters is $\lesssim 1$.

To better appreciate the fractal distribution of H_2O masers, it is instructive to compare it with models of homogeneously distributed random points. In our numerical model we created 90 points randomly and uniformly distributed in a thin spherical shell and then projected this distribution onto a plane. A drastic difference between the model distribution and the observed maser distribution can be seen visually (a lack of clustering in the model distribution) and is confirmed by the measured spatial dimension of the model point sets. As anticipated, both box-counting and density-radius methods gave $d \approx 2$ for the random, homogeneous cluster of model dots, to be compared with $d \lesssim 1$ for the observed clusters of maser spots.

Other types of masers should also be tested for possible fractal structure. At least some of them do not seem to have such structure. For example, the OH masers associated with regions of star formation do not show self-similar spatial distribution; rather, they demonstrate strong clustering on one scale, $\sim 10^{15}$ cm (Reid et al. 1980). These masers form just outside an expanding ultracompact H II region and would not be expected to have a turbulent structure of the same kind as the H_2O masers that are due to the shear between a stellar wind and surrounding gas (see § 6).

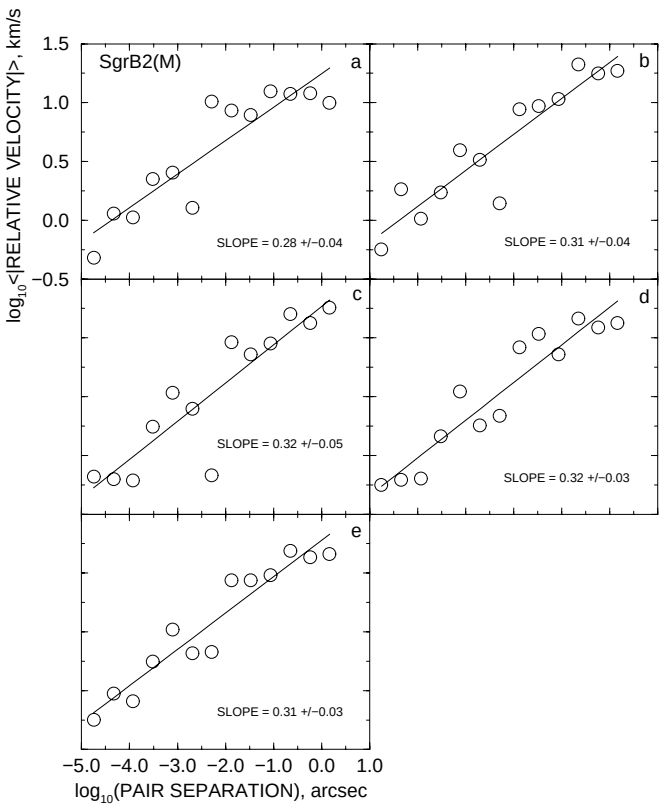

FIG. 5.—Two-point line-of-sight velocity correlation function for H_2O masers in Sgr B2(M). The open circles represent data, and the straight solid line shows a linear fit. (*a*)–(*d*) Results for the four epochs of observation; (*e*) average for the four epochs.

4. STATISTICS OF THE VELOCITY FIELD

We investigated two statistical properties of the velocity field traced by H_2O masers in the same five sources: (1) the low-order two-point velocity structure functions and (2) the probability distribution for the deviations of the two-point velocity increment from its mean value at different spatial scales.

4.1. *Two-Point Velocity Structure Functions*

Most statistical studies of the kinematics and structure of interstellar gas using masers as probes have so far been limited to one velocity component (the line of sight) and two coordinates on the celestial sphere. Owing to the smallness of maser sources (a whole source is only $\sim 1''$ across), the two spherical celestial coordinates are, with high precision, approximated by rectangular Cartesian coordinates. We assume, as all previous authors implicitly did, that if a power-law scaling relation exists for velocity vectors in three-dimensional space, the same relation, with the same exponent, holds for the dependence of the line-of-sight component of velocity on projected distances. This is a reasonable assumption if the velocity field is isotropic. It is analogous to the well-known use of the longitudinal velocity component in incompressible turbulence studies (see, e.g., Frisch 1995).

Statistical analysis of the velocity field probed by H_2O masers has previously been performed for W49N on two independent sets of data (Walker 1984; Gwinn 1994). We discuss here only the low-velocity H_2O maser spots (approximately ± 20 km s^{-1} from the systemic velocity), which are more likely connected with the "Kolmogorov-type" supersonic turbulence than the high-velocity spots (§ 6). Walker (1984) did not see an explicit dependence of two-point velocity increments on point separation for low-velocity features, shown in his Figure 8. One can interpret this graph as a power law with the exponent $q \lesssim 0.2$. Gwinn (1994) found $q \approx 0.33 \pm 0.01$ for the dependence of the median velocity differences on the one-dimensional projection of the maser pair separation. One can conclude from these two studies that the value of q for the two-point correlation function in W49N/H_2O does not surpass $\frac{1}{3}$.

For each of the five H_2O sources (§ 3) we calculated the structure functions

$$D_\alpha(l) \equiv \langle |v(\boldsymbol{r}) - v(\boldsymbol{r} + \boldsymbol{l})|^\alpha \rangle \qquad (7)$$

for low values of the order of the function, $\alpha = 1\text{–}3$. In equation (7) the vectors $\boldsymbol{r}$ and $\boldsymbol{l}$ determine the positions of the two points in the plane of the sky, while v designates the line-of-sight velocity and l the two-dimensional projection of the linear distance between the points. Our calculation procedure is as follows. The whole range of maser spot angular separations (up to 4 orders of magnitude, in both sources) is divided into N bins, with logarithmically increasing bin size and thus logarithmically increasing separation between bin centers. Using the VLBI relative position data, the procedure selects all pairs within a given separation bin and calculates one of the functions (eq. [7]). This procedure

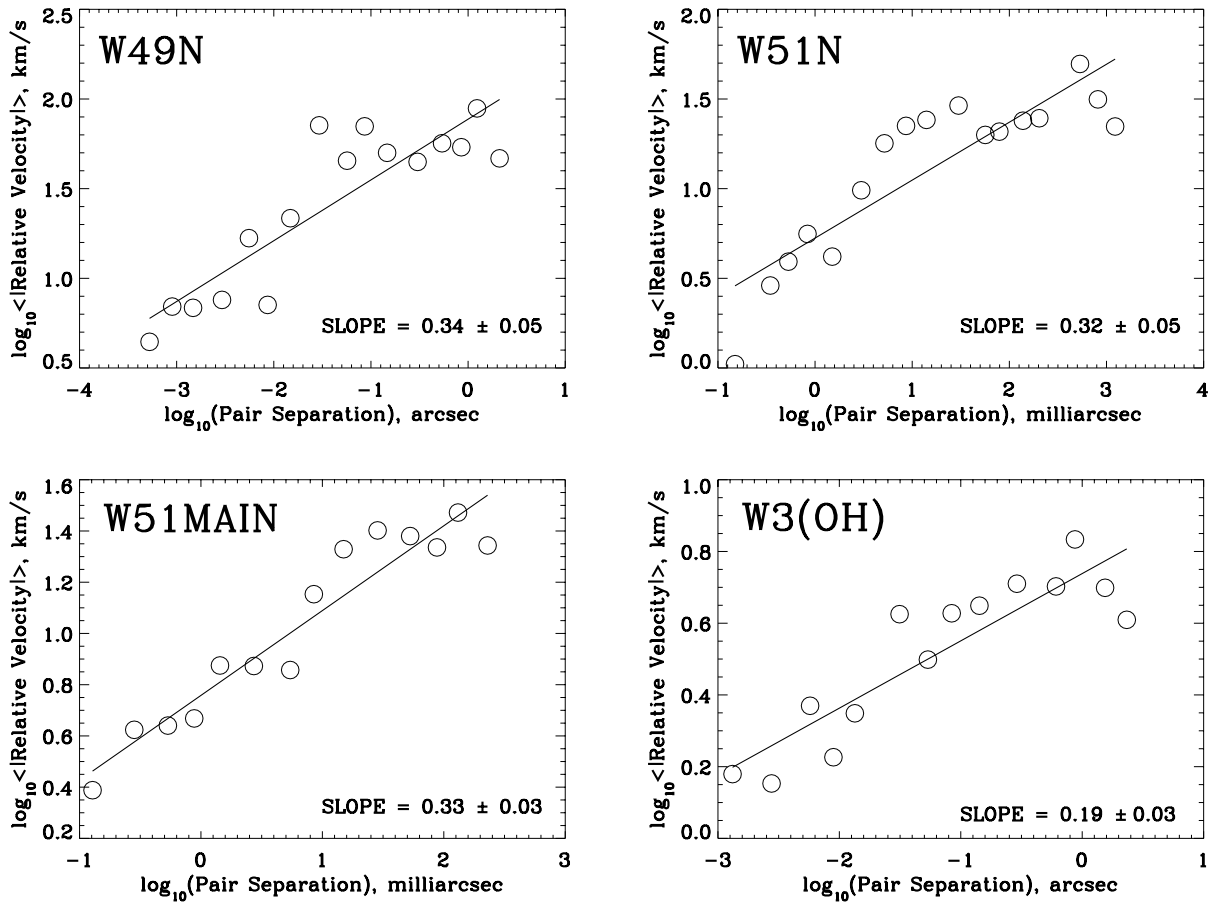

FIG. 6.—Two-point line-of-sight velocity correlation function for H_2O masers in W49N, W51N, W51MAIN, and W3(OH)

is repeated for every separation bin, and the resultant averages of the powers of velocity differences are plotted as a function of separation in a log-log graph. A least-squares fit of a straight line to the points on the graph is then performed to obtain a power-law exponent q and its uncertainty ($1\,\sigma$).

Figure 5 gives the results for Sgr B2(M), for $\alpha = 1$. The figure shows the results for the four epochs of observations

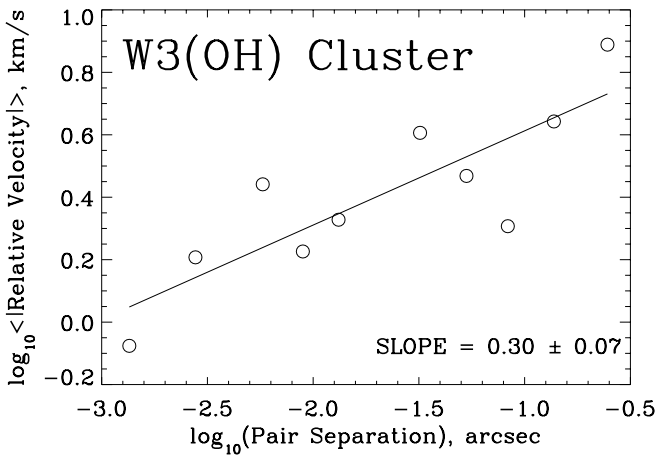

FIG. 7.—Two-point line-of-sight velocity correlation function for H_2O masers in one of the two "clusters" (streams of bipolar outflow) in W3(OH).

(§ 2), as well as their average. The data are satisfactorily approximated by a power law. We obtain $q = 0.31 \pm 0.03$ when the whole set of data is used. When data for the largest scales ($\log|\Delta\theta\ (\text{arcsec})| \geq -0.5$) are excluded (to avoid possible edge effects), the value of q changes insignificantly: $q = 0.34 \pm 0.03$. The second- and third-order structure functions have the exponents of 0.62 ± 0.06 and 0.93 ± 0.09, respectively. We note that for all three structure functions the power-law exponents are close to their classic Kolmogorov values, which are $\frac{1}{3}$, $\frac{2}{3}$, and 1.0 for $\alpha = 1$, 2, and 3, respectively.

The results for $\alpha = 1$ for other sources are presented in Figure 6. The power-law approximation gives the values of q close to $\frac{1}{3}$ for all the sources except W3(OH), where it is significantly lower (0.19 ± 0.03). In this source, however, the VLBI map reveals a strong regular component of motion (strongly collimated bipolar outflow), which should significantly influence the results when the whole VLBI map is considered for the statistical analysis. To decrease the influence of the regular velocity component, we obtained the first-order structure function for only one of the two lobes of the bipolar outflow. In this case, the regular component of the relative velocities should be minimal, and one can anticipate that the bulk of the relative motions of the condensations will be due to turbulence. The result is shown in Figure 7; the value of q (0.30 ± 0.07) is now much closer to the Kolmogorov value.

With all sources displaying the low-order structure functions close to Kolmogorov's, one might wonder how likely

it is that this is simply coincidental. Can regular, nonturbulent velocity fields, such as expansion and/or rotation, produce the observed power-law dependence of the velocity increments on spatial scales, with the power index close to $\frac{1}{3}$?

In order to answer this question, we applied the same statistical analysis to the results of numerical modeling that simulated regular motions of the maser spots only. A total of 90 model dots were randomly and uniformly distributed in a thin spherical shell. Three types of regular motion were considered: (1) radial expansion, (2) rotation around an axis perpendicular to the line of sight, and (3) expansion plus rotation. In the last case we varied the ratio of the absolute values of the expansion velocity and the velocity of rotation on the equator.

The results of the line-of-sight velocity versus dot separation correlation analysis are shown in Figure 8. The long straight line on the plots shows the slope $\frac{1}{3}$ for reference. The quickly growing dispersion of the data points at smaller scales, seen on all the plots, is due to the uniform, nonfractal distribution of the points: a lack of clustering, and thus poor statistics, at smaller scales. This large dispersion makes a linear fit beyond about 1.5 orders of magnitude from the largest scale meaningless. The slope of the fitting line, drawn in this limited interval, changes from about zero for the case of pure expansion ($\approx 0.08 \pm 0.02$, for the specific realization shown in Fig. 8) to approximately unity for the case of pure rotation (1.01 ± 0.01 in the example shown). All intermediate values of the slope can be achieved by combining expansion and rotation in a due proportion (*four lower panels*). In particular, the "Kolmogorov" value $\frac{1}{3}$ is achieved when the ratio of the velocity of rotation on the equator to the velocity of expansion is ≈ 3.

It is quite improbable, however, that this ad hoc combination of kinematic parameters plus the same orientation of the axis of rotation is realized in all the sources under study. In all the published models of the observed proper motions and radial velocities of H_2O masers the deduced model ratio of the expansion to rotation velocities is greater than 1. In W49N these velocities are almost equal: 17 and 16 km s^{-1}, respectively (we consider here only the low-velocity component of expansion; see § 6). It is seen from Figure 8 that such a high ratio of expansion to rotation should produce a flatter slope than $\frac{1}{3}$ at large scales. It is noteworthy that flattening of the slope of the two-point correlation function does indeed appear at larger scales for all the sources in Figure 6. This reveals the contamination of the statistical properties of the turbulent component of motion by the regular component. The role of the regular component(s) of the velocity field relative to the turbulent component drops with the decreasing spatial scale, and it is remarkable how effectively the smaller scales "compensate" for the flattening at the larger scales in Figure 6 and force the average slope to tend to its Kolmogorov value.

4.2. *Statistics of Deviations from the Mean Velocity Increment*

An inherent manifestation of terrestrial turbulent flows is *intermittency*, i.e., the spatial and temporal inhomogeneity of the velocity field. Intermittency results in enhanced, higher than Gaussian, probability of large deviations of the two-point velocity increments from their average value at a given spatial scale. Deviations from a Gaussian distribution have been observed in laboratory and atmospheric incompressible turbulent flows (Dutton & Deaven 1969; van Atta & Park 1972). Falgarone & Phillips (1990) and Falgarone, Phillips, & Walker (1991) attributed the broad (broader than Gaussian) wings of the emission-line profiles observed in molecular clouds to an excess of large deviations from the average velocity difference in the cloud.

H_2O masers are more direct probes of the velocity field than thermal molecular lines observed in the cold clouds (see § 6). Typically, the available VLBI results provide coordinates and line-of-sight velocities for $n \approx 100$ maser spots per observation. Thus, there are $m = n(n-1)/2 \approx 5000$ unique pairings for measuring the velocity difference distribution. Given this relatively large number, we hoped that the statistics were sufficient to identify possible deviations from a Gaussian distribution at various spatial scales. Figures 9 and 10 show examples of velocity difference probability distributions obtained for particular spatial ranges in Sgr B2(M). The range for a given spatial scale was chosen to be equal to the scale. Unfortunately, some individual distributions were found to be not well-defined, centrally peaked distributions, which is evidently due to insufficient statistics.

In order to produce a more statistically significant result, we attempted to co-add the individual distributions. The summation was done as follows. The velocity difference (x-axis) and the number of pairs or counts (y-axis) of the individual distributions were independently normalized. The y-axis was normalized by dividing all bin counts by the maximum bin count. In order to normalize the x-axis, we first considered how the absolute value of the maximum velocity difference of individual distributions scaled as a function of radial separation between maser pairs. We found that this function was well approximated by a power law. The best-fitting straight line gave the exponent $\approx \frac{1}{3}$. Given the previously established Kolmogorov scaling law for the mean

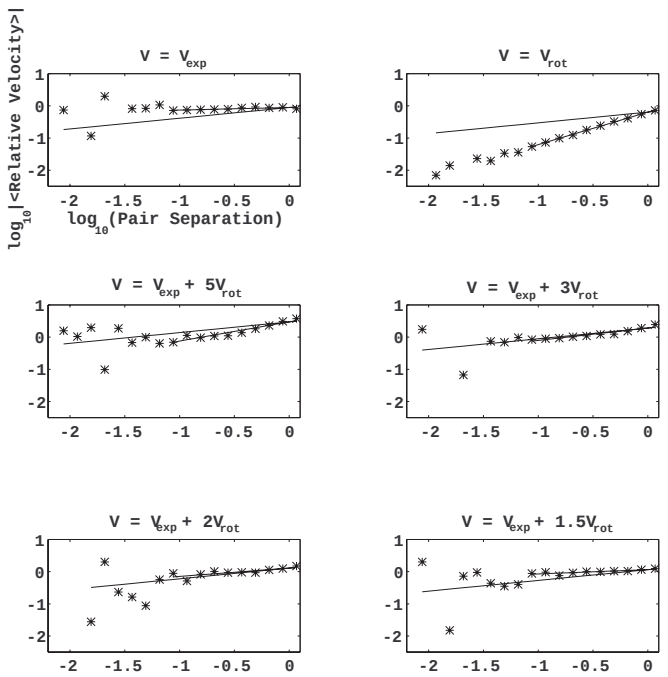

FIG. 8.—Two-point line-of-sight velocity correlation function for a planar projection of a randomly filled spherical shell, for different ratios of expansion and rotation components. Asterisks represent data. One of the two straight lines in each graph shows a linear fit (possible only for the largest scales); the other line indicates, for reference, a slope of $\frac{1}{3}$.

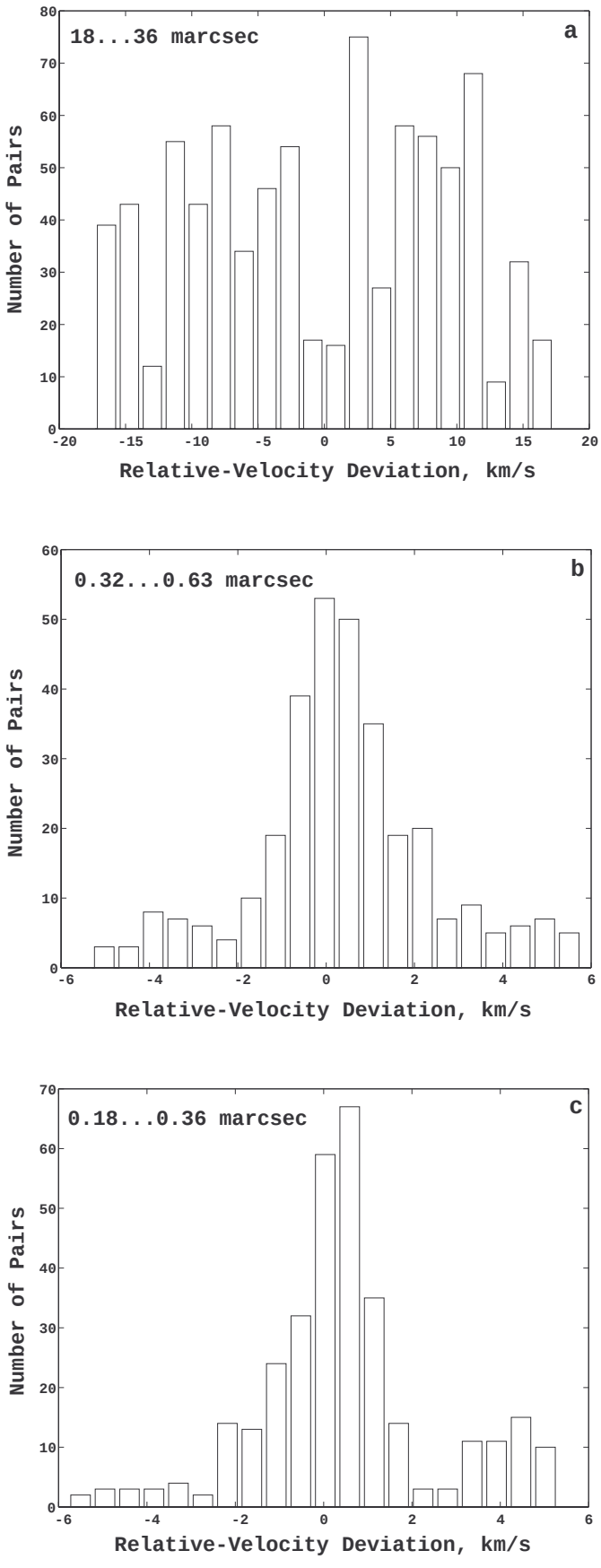

FIG. 9.—Histograms of the number of pairs having a given value of the deviation of their relative velocity from its mean value. (*a*) Separation range 18–36 mas; (*b*) separation range 0.32–0.63 mas; (*c*) separation range 0.18–0.36 mas.

absolute velocity differences between maser points, this result could be anticipated if we assume that the dispersion of velocity differences at a given scale is proportional to the mean absolute velocity difference at that scale. Using the resulting linear fit, the dispersions of velocity differences for individual distributions were normalized by multiplying the x-values of a distribution by the ratio $\Delta v^0_{\max}/\Delta v^l_{\max}$, where $\Delta v^0_{\max}$ is arbitrarily chosen to equal the maximum observed absolute value of the velocity difference occurring in the central spatial bin and $\Delta v^l_{\max}$ is the maximum absolute velocity difference value of an individual distribution. Once the x- and y-axes of the individual distributions were normalized, these distributions were co-added, producing a single histogram of the distribution averaged over spatial scales.

The conjoined histogram for Sgr B2(M) is shown in Figure 10. It has a well-defined, centrally symmetric shape. However, fitting it with a single Gaussian results in strong positive residuals in the wings of the distribution (Fig. 10*a*). A two-Gaussian fit, both Gaussians being centered at zero, results in much smaller residuals (Fig. 10*b*). Because of the method by which this histogram has been obtained, it contains only averaged (over all the spatial scales) information about the probabilities of deviations. Comparing the conjoined histogram with the individual histograms shows that summation significantly improves the statistics. This is indirect evidence that the velocity field at all or most of the accessible spatial scales has qualitatively similar statistical properties, including an excess of large deviations from Gaussian distribution. The two-Gaussian fit of the conjoined distribution provides a quantitative measure of the excesses, averaged over the entire scale range. The narrower Gaussian approximately describes the central part of the distribution, and the broader one describes its wings. The ratio "narrow/broad" of areas under these two Gaussians measures the excess of large deviations. From Figure 9*b*, this ratio is ≈ 0.63, considerably less than unity. Thus, the super-Gaussian wings are indeed significant.

Figure 11 shows the results of the same analysis for four other H_2O sources. In all of them, the wings of the distribution are much broader than those of the Gaussian that fits the central part of the distribution. This demonstrates that excess of large velocity difference deviations is a common feature of the turbulent velocity fields probed by H_2O masers.

5. IMPLICATIONS FOR SUPERSONIC TURBULENCE

In this section we discuss possible implications of our results for the theory of supersonic turbulence. The statistical study of H_2O masers described in the previous sections reveals three important results: (1) self-similarity (fractality) of the spatial distribution of the maser spots; (2) power-law character of the structure functions for the velocity field traced by the masers, with the power indices close to their classic Kolmogorov values for incompressible turbulence; and (3) excess of large fluctuations of the two-point velocity increments. As all these features are typical of the relatively well studied, incompressible turbulence, one can suspect that H_2O masers in regions of star formation arise in a turbulent medium. If this assumption is correct, H_2O masers, as a result of their record brightness and small angular sizes, may become unique probes of astrophysical turbulence. Since the velocity increments at the largest scales in the H_2O clusters are much greater than the probable speed of sound in neutral molecular gas, we deal here, by definition, with the

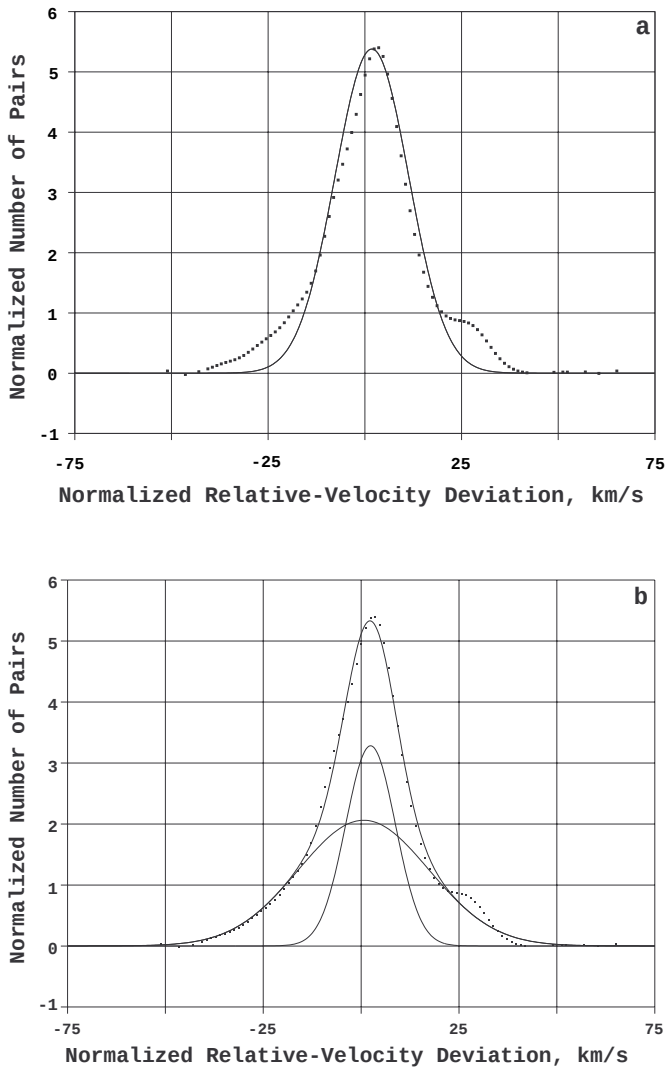

FIG. 10.—Probability of deviation of the two-point velocity difference from its mean value, averaged over scales for the H_2O maser spots in Sgr B2(M). Both abscissa and ordinate axes are normalized as described in text. Dots represent data. Solid lines show (*a*) a one-Gaussian fit and (*b*) a two-Gaussian fit to the data points.

poorly studied supersonic regime of turbulence. Comparison with the available theoretical knowledge about incompressible turbulence should therefore be done with caution.

5.1. *Fractal Dimension and Intermittency of Turbulence*

The major conclusion of our analysis in § 3 is that the spatial distribution of H_2O masers is fractal and that the measured fractal dimension is low, $d \lesssim 1$. If H_2O masers trace the dissipation of supersonic turbulence, we should conclude that the fractal dimension of supersonic turbulence is considerably lower than that of incompressible turbulence, the latter being ≈ 2.6 (Mandelbrot 1982). If one accepts the hypothesis that mass fluctuations in star-forming clouds are produced by supersonic turbulence (Larson 1995), then the low fractal dimension (≈ 1.4) of a cluster of young stars in Taurus measured by Larson can be considered as a corroboration of our conclusion. Another relevant fact may be the observed low fractal dimension of the large-scale distribution of galaxies ($d \approx 1.2$; Mandelbrot 1982), but the role of turbulence in shaping this structure is even less clear.

It is helpful to introduce the "running" filling factor, β, of "daughter" turbulence elements within "mother" elements (Frisch 1995). The dimension of a fractal is expressed through β by

$$d = d_0 - \frac{\ln \beta}{\ln s} , \tag{8}$$

where d_0 is the dimension of the supporting space and $s < 1$ is the scaling factor from the mother eddies to the daughter eddies. Constancy of β from scale to scale guarantees a well-determined value of d (a linear plot in Figs. 2–4). From equation (8)

$$\beta = s^{d_0 - d} , \tag{9}$$

which shows that the filling factor of active daughter eddies in mother eddies decreases when the fractal dimension of turbulence decreases. The filling factor of active eddies is a direct measure of the degree of intermittency (spottiness) of turbulence. We conclude that highly supersonic turbulence, as revealed by H_2O masers and perhaps by the large-scale galaxy distribution and the distribution of stars in young clusters, is more intermittent than incompressible turbulence.

The very possibility of representing the observed spatial distribution of active turbulence elements by a single power law means that turbulence is intermittent on virtually all scales. The all-scale intermittency is also corroborated by the fact that the strong excess of the large velocity difference deviations is revealed by the statistics averaged over different spatial scales (§ 4.2). This seems to be an important conclusion because, in the case of incompressible turbulence, with its relatively high fractal dimension, the existence of intermittency in the inertial subrange of the scales (as opposed to the dissipation subrange) has long been an open question (Frisch 1995).

5.2. *Does Supersonic Turbulence Have an Inner Scale?*

According to the classical work by Kolmogorov (1941b, 1941c), incompressible turbulence is characterized by two limiting scales: the outer scale L, where energy is supplied to the turbulent flow, and the inner scale η, where it is dissipated via molecular viscosity. The "inertial" subrange of linear scales l, where kinetic energy is neither injected into turbulence nor dissipated, but only transferred from larger to smaller scales, is between $L \gg l \gg \eta$. In the inertial subrange, turbulence tends to become homogeneous and isotropic. Kolmogorov demonstrated that the inner scale of incompressible turbulence is of the order of

$$\eta_i \sim \left(\frac{\nu^3}{\bar{\epsilon}} \right)^{1/4} , \tag{10}$$

where ν is the kinematic viscosity of the fluid and $\bar{\epsilon}$ is the mean rate of energy dissipation per unit mass, given by

$$\bar{\epsilon} = \frac{U^3}{L} , \tag{11}$$

where U is the characteristic velocity difference at the outer scale L. The expression given by equation (10) for the dissipation scale is readily obtained from dimensional considerations; it is the only combination with the dimensions of length that can be constructed from the two parameters relevant to this mechanism of energy dissipation, ν and $\bar{\epsilon}$.

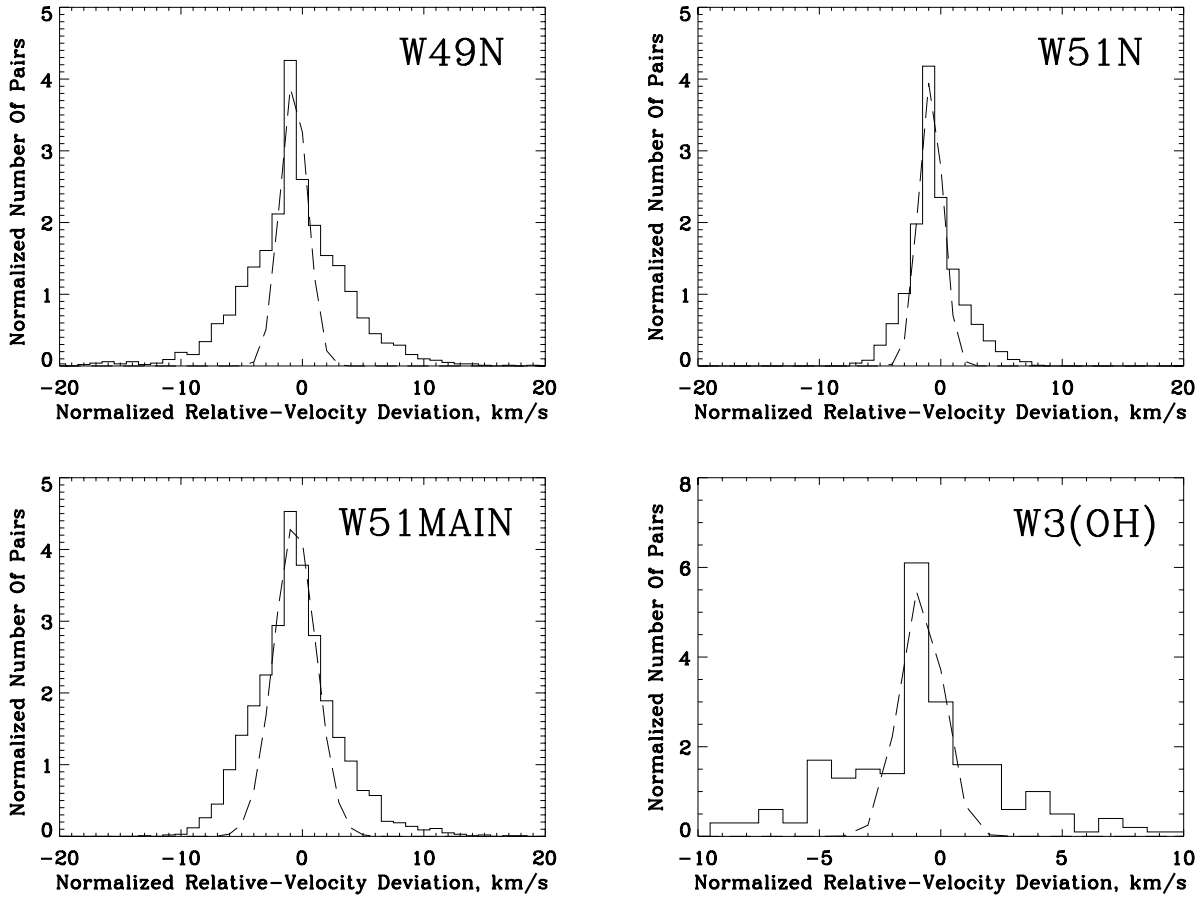

FIG. 11.—Same as in Fig. 10, but for H_2O masers in W49N, W51N, W51MAIN, and W3(OH) ("Cluster"). *Solid line:* observed data; *dashed line:* one-Gaussian fit to the central part of the observed distribution.

Our attempt to derive a possible inner scale for highly supersonic turbulence is based on two assumptions. First, proceeding from the common belief that the major mechanism of energy dissipation in supersonic turbulence is via shock waves, we assume that the sonic speed, c_s, rather than the molecular viscosity, is the relevant parameter of the problem. Our second assumption may be more arguable. We assume that the second relevant parameter of the problem is the same as for incompressible turbulence: the mean rate of energy dissipation, $\bar{\epsilon}$. Thus, we assume that $\bar{\epsilon}$ is an approximate constant of the energy cascade, equal to the rate, per unit mass, of supply of kinetic energy at the outer scale. In other words, we assume no significant energy dissipation at intermediate scales. Although some theoretical and observational arguments can be provided in favor of this hypothesis (see below), we emphasize that, for the moment, it is only a hypothesis, whose consequences we would like to compare with observations.

With these two assumptions, we can derive the dissipation scale for supersonic turbulence, η_s, using standard dimensional analysis. It is easy to show that only one combination can be formed by c_s and $\bar{\epsilon}$ with the dimensions of length, namely,

$$\eta_s \sim \frac{c_s^3}{\bar{\epsilon}} \ . \tag{12}$$

Substituting $\bar{\epsilon}$ from equation (11) into equation (12), we can give η_s a more useful form:

$$\eta_s \sim \frac{c_s^3 L}{U^3} = \frac{L}{M_L^3} \ , \tag{13}$$

where $M_L = U/c_s$ is the typical value of the Mach number associated with the outer scale. Equation (13) shows that in highly supersonic turbulence ($M_L \gg 1$), the scale where shock waves begin to dissipate turbulent energy effectively is many orders of magnitude smaller than the outer scale L.

An argument in favor of our assumption that highly supersonic turbulence does not dissipate much of its kinetic energy at larger scales is the observed Kolmogorov, $\frac{1}{3}$, slope of the two-point velocity correlation function in H_2O masers. The $\frac{1}{3}$ slope is a straightforward consequence of the conservation of energy during its cascade along the hierarchy of scales. Any energy dissipation in the inertial subrange would produce a steeper slope. The specific kinetic energy associated with turbulent pulsations on a linear scale l is $\sim v_l^2$, where v_l is the rms turbulent velocity on the scale l. This energy is passed to smaller scales in about one "turnover" time,

$$\tau \sim \frac{l}{v_l} \ . \tag{14}$$

Therefore, the rate of energy transfer is

$$\bar{\epsilon} \sim \frac{v_l^2}{\tau} \sim \frac{v_l^3}{l} \ . \tag{15}$$

If $\bar{\epsilon}$ is constant, equation (15) gives $v_l \propto l^{1/3}$.

Suppose now that some amount of energy is dissipated on each scale. Then $\bar{\epsilon}$ is not a constant: it decreases with decreasing l. Approximating this decrease by a power law,

$$\frac{v_l^3}{l} \propto l^{\alpha} , \quad \alpha > 0 , \tag{16}$$

we have

$$v_l \propto l^{(1/3)(1+\alpha)} , \tag{17}$$

which demonstrates the steeping of the scaling law (since $\alpha > 0$).

Why can energy dissipation in larger scale shocks be hindered in highly supersonic turbulence? Here is one possible answer. Although the potential component of the velocity field (describing compression and expansion of the gas) should play some part in a supersonic flow, this part may crucially depend on the unknown boundary and initial conditions of the flow (e.g., Falgarone et al. 1994). An extreme case is a purely vortical initial motion of gas at the larger scales. In this case, although the velocity increments for these scales (the difference in velocities of two opposite peripheral points of an "eddy") may be highly supersonic, most converging flows within the eddy, which arise from fluctuations, will produce *oblique* shocks, whose normal velocity component, $v_{\rm sh}$, will not exceed c_s by much, and thus it will be small in comparison with the average vortical velocity increment: $v_l \gg v_{\rm sh} \sim c_s$. Thus, even if a shock of large scale is formed, the time it needs to sweep the eddy and dissipate its kinetic energy is much longer than the turnover time (given in eq. [14]), during which the eddy will disintegrate, passing its energy to smaller scales. Only when v_l drops down to $\sim c_s$, which happens at the inner scale, do v_s and v_l become comparable, and massive dissipation of kinetic energy in random shocks becomes possible. This gives a possible physical justification to equation (13).

5.3. *Intermittency and Kolmogorov Spectrum*

The important conclusion from the results presented in § 4.1 is that the exponents of the low-order structure functions for the highly supersonic turbulence are close to their classic Kolmogorov values. In particular, the exponents of the second-order structure function in all the investigated sources are close to $\frac{2}{3}$. This value was predicted by Kolmogorov for homogeneous incompressible turbulence at very high Reynolds numbers (Kolmogorov 1941a, 1941b, 1941c). Later, many authors, beginning with Kolmogorov himself (Kolmogorov 1962), attempted to introduce theoretical corrections to this exponent that would account for the experimentally detected intermittency of turbulence (e.g., Mandelbrot 1967; Frisch, Sulem, & Nelkin 1978; see also Frisch 1995). For example, in the popular "β-model" of Frisch, Sulem, and Nelkin, intermittency is assumed to have a fractal geometry, and the corrected exponent is given by

$$\zeta_2 = \frac{2}{3} + \frac{3-d}{3} , \tag{18}$$

where d is the fractal dimension of the set on which intermittent turbulence concentrates. In the case of incompressible turbulence $d \approx 2.6$–2.8; therefore, the codimension $3-d$ and the whole correction factor (second term in eq. [18]) are small. In fact, most of these intermittency corrections have historically been introduced as *small* parameters, to account for the small degree of observed intermittency in incompressible flow. This has made it difficult to discriminate between different theoretical models, as well as to judge, in general, the plausibility of the approach treating intermittency as a "disturbance" to the classic Kolmogorov theory.

Highly supersonic turbulent flow should have specific features different from those of incompressible turbulence. These two regimes of turbulence should, at least, differ in the ways they ultimately dissipate energy: via shock waves and molecular viscosity, respectively. However, the power-law character of the observed spectrum of supersonic turbulence, over several decades in scale, is a strong indication that the energy cascade from larger to smaller scales is as intrinsic a property of supersonic turbulence as it is for incompressible turbulence. Moreover, the prominent fractal structure of the set on which supersonic turbulence dissipates its energy and the non-Gaussian statistics of the two-point velocity increments, as revealed by H_2O masers, are strong evidence for qualitative similarity of both regimes of turbulence also in the sense of an intermittent character of turbulent activity.

Since the energy cascade and intermittency are the only two assumptions in the above-mentioned models of incompressible turbulence, these models should likely also work in the case of supersonic turbulence. The only application of incompressibility of turbulence in these models is the assumption that energy is not dissipated at the intermediate (inertial subrange) scales. This assumption is not obvious for compressible, supersonic turbulence. However, the observed slope of the two-point velocity correlation function, close to Kolmogorov's, suggests that dissipation on intermediate scales is insignificant in the supersonic case, too (§ 5.1).

It is important to note, in this connection, that the H_2O masers reveal a very low fractal dimension ($d \lesssim 1$) of the set on which supersonic turbulence ultimately dissipates in shock waves. With such a low d, the correction term from the β-model (eq. [18]) is large, and we anticipate that, as a result of intermittency, the slope of the second-order structure function will be at least twice as steep as Kolmogorov's classic value. Any dissipation of energy on intermediate scales (the only possible difference from the incompressible case) would steepen the structure function even more. However, the observed structure functions are close to Kolmogorov's.

The observed pronounced intermittency of turbulence combined with the classic Kolmogorov velocity structure functions can only be understood if we accept that intermittency is inherent in turbulence, not a mere disturbance of its classic Kolmogorov properties. Such an approach to incompressible turbulence is being developed by Barenblatt & Chorin (1997, hereafter BC97). These authors claim, in particular, that both the tendency of the second-order structure function to its classic dependence on l and an increase of the degree of intermittency are natural asymptotic properties of turbulence when the Reynolds number tends to infinity.

As first pointed out by von Weizsäcker (1951), the Reynolds numbers of the interstellar gas are, in general, very high. The Reynolds numbers of the dense nuclei of the star-forming molecular clouds, where H_2O masers reside, are especially high, as a result of the low viscosity of the dense gas. The turbulent flows probed by H_2O masers have typical velocities $U \sim 10^6$ cm s^{-1} at a scale of $L \sim 10^{17}$ cm.

With the typical number density $\sim 10^6$ cm^{-3} and temperature $\sim 10^2$ K for a molecular cloud core, the kinematic viscosity is $\sim 10^{13}$ cm^2 s^{-1}, and the typical value of the Reynolds number, $\mathrm{Re} \equiv LU/\nu$, is $\sim 10^{10}$.

For incompressible turbulence, the Reynolds number is a measure of the width of the inertial subrange. If the inertial subrange of supersonic turbulence probed by H_2O had been limited by viscosity, it would have been very large. However, there is little doubt that, in the highly supersonic regime, the dissipation of energy starts at a much larger scale than the inner scale determined by viscosity. In § 5.2 we postulated the existence in highly supersonic turbulence of an inner scale determined by energy dissipation in small-scale stochastic shocks and given by equation (13). Although this inner scale is much larger than the Kolmogorov dissipation scale ($\eta_s \sim 10^{13}$ cm; $\eta_i \sim 10^7$ cm), there is still a large inertial subrange in the highly supersonic regime: almost four decades in projected linear scale.

One can try to reformulate the BC97 theory and obtain an asymptotic law for the supersonic regime using the Mach number rather than the Reynolds number. As is customary in crude phenomenological approaches, we shall ignore distinctions between structure functions involving different components of the velocity vectors. Specifically, we shall assume that the second-order structure function D_{zz} involving the line-of-sight (z) component of the difference velocity vector for two points reflects typical properties of all other structure functions.

Following the reasoning of BC97, we can assume that in the inertial subrange of supersonic turbulence

$$D_{zz} = f(l, L, \bar{\epsilon}, c_s) \, , \tag{19}$$

where $\bar{\epsilon}$ is the mean rate of energy dissipation per unit mass. It is assumed that in this inertial subrange the energy flux from larger to smaller scales is nearly constant and equal to $\bar{\epsilon}$. Applying the standard dimensional analysis, we find the scaling law for D_{zz}:

$$D_{zz} = (\bar{\epsilon} l)^{2/3} \Phi\left(\frac{l}{\eta_s}, M_L\right) \, , \tag{20}$$

where Φ is a dimensionless function of its two dimensionless arguments. We chose the Mach number at the outer scale, M_L, and the running scale l measured in the units of inner scale, η_s, as the two dimensionless arguments. In the case of incompressible turbulence the Reynolds number, instead of the Mach number, enters the parentheses in equation (20).

The dimensional analysis, by itself, does not tell us anything about the properties of the function Φ and its two arguments. In order to finalize the scaling law, one must make a *similarity assumption* about the behavior of Φ as its two arguments tend to infinity. As BC97 point out, two different assumptions about this function mark the historical evolution of incompressible turbulence theory:

1. Complete similarity in both arguments: $\Phi \approx \Phi(\infty, \infty) = \mathrm{const}$, when both dimensionless arguments tend to infinity (Kolmogorov 1941a).
2. Complete similarity in Re, but incomplete similarity in l/η, leads to a power-law dependence of Φ on l/η (Kolmogorov 1962).

The first assumption leads to the classic Kolmogorov $D(l) \propto l^{2/3}$. The second assumption introduces an additive correction to the power index, which has been interpreted as a correction for intermittency. BC97 argue that the second assumption is internally contradictory and make the separate assumption of incomplete similarity in l/η and *no* similarity in Re. This again generates an additive correction to the power index, but now the correction depends on the value of Re. In the limit of $\mathrm{Re} \to \infty$ the correction tends to zero and one is left with the classic $D(l) \propto l^{2/3}$ dependence. The correction is substantial only when Re is not large.

These similarity arguments can be repeated in the case of highly supersonic turbulence, with the formal substitution of M_L for Re. The BC97 theory makes no quantitative estimates of the magnitude of Re (or M_L, in our case) necessary to reach the asymptotic behavior of D. We can suppose that in the case of turbulence probed by H_2O masers, M_L is high enough for the correction to Kolmogorov value of the power index to lie within the experimental errors. Thus, the BC97 theory (and its extension to supersonic turbulence) rejects the notion that significant intermittency requires a significant correction to Kolmogorov's (1941a, 1941b, 1941c) law and thereby reconciles the observed low fractal dimension (high intermittency) of supersonic turbulence and its classic Kolmogorov velocity structure functions.

6. THE ORIGIN OF H_2O MASERS

One can speculate that a jet from a young star produces two basic flow regimes in the ambient gas: (1) a frontal, high-Mach shock and (2) a high-vorticity flow due to the velocity shear at the side interface of the jet and the ambient gas (e.g., Masson & Chernin 1993). We surmise that the low-velocity H_2O masers are associated with the second regime. The high-velocity H_2O masers may be connected with the first regime, but one can anticipate that this connection, and turbulence produced by the frontal shock, would be more complicated than in the second regime. Looking for the simplest cases of supersonic turbulence, we discuss only the second regime and the low-velocity masers in this investigation.

A power-law spatial distribution correlation function in all of the H_2O sources investigated here signifies self-similar clustering over almost 4 orders of magnitude in scale, from $\sim 10^4$ to ~ 1 AU. The "minimal clusters" in this hierarchy ("features" in the terminology of Gwinn 1994) are actually spatial and spectral blends of elementary sources, i.e., those observed through an element of spectral resolution. By the order of magnitude, both the elementary sources and the minimal clusters have a typical size of ~ 1 AU, which is intriguingly close to the predicted dissipation scale of supersonic turbulence, given by equation (13). In a typical H_2O maser source, the low-velocity features are spread over a projected area of $L \sim 10^{17}$ cm and occupy a velocity interval $U \approx 20$ km s^{-1}. Taking $c_s \approx 1$ km s^{-1} (appropriate for probable kinetic temperatures of several hundred K), we have $M_L \approx 20$ and $\eta_s \sim 10^{17}/(20)^3 \sim 10^{13}$ cm ~ 1 AU. Unless this is a coincidence, the smallest clusters of H_2O masers may be the sites of the ultimate dissipation of turbulent energy via stochastic shocks on the inner scale of supersonic turbulence.

This new conceptual approach to H_2O masers may have several important consequences for understanding the very mechanism of masing in these sources. It has often been argued that shock waves provide the best conditions for pumping H_2O masers. Strelnitski & Sunyaev (1973) interpreted the observed large dispersion of the H_2O Doppler

velocities in W49N as due to supersonic gas outflow from a young host star and conjectured that the interaction of the outflow with the surrounding gas could produce shock waves necessary for pumping. This hypothesis has been further developed by many authors, who have elaborated on details of the shock structure and collisional-radiative (the first word standing for the source and the second for the sink of the quantum heat engine) or collisional-collisional schemes of maser pumping behind a shock (e.g., Shmeld, Strelnitski, & Muzylev 1976; Strelnitski 1984; Kylafis & Norman 1986, 1987; Hollenbach, McKee, & Chernoff 1987; Elitzur, Hollenbach, & McKee 1989; Kaufman & Neufeld 1996). A common feature of all these models is that the pumping shock is a result of a direct collision of the outflow with a dense blob in the surrounding quiescent gas or a direct collision of a dense blob in the outflow with the surrounding gas (Tarter & Welch 1986). In the present model, the pumping energy is not imparted to the masing gas blobs directly by the stellar wind. Instead, the energy is channeled to the masers by a cascade from larger scales, which receive energy from the stellar wind or jets.

In previous models, the shocks pumping H_2O masers were assumed to have high velocities. These were either high-speed ($\gtrsim 50$ km s^{-1}) dissociative J-type shocks (Elitzur et al. 1989) or slower ($\gtrsim 10$ km s^{-1}) C-type shocks propagating perpendicular to the magnetic field (Kaufman & Neufeld 1996). Two main goals were pursued in developing those models: (1) the achievement of the maximum possible abundance of H_2O molecules via chemical reactions and (2) the realization of sufficiently high kinetic temperatures for pumping the 6_{16}–5_{23} and other masing transitions. It has been argued (Melnick et al. 1993; Kaufman & Neufeld 1996) that to fulfill both these requirements, temperatures $\gtrsim 1000$ K are needed. An important question is whether the slow shocks we advocate in this paper can provide such temperatures. An analysis of the shock structure is beyond the scope of the present paper. However, we note that a J-type shock propagating *along* the magnetic field lines will have a postshock temperature $\gtrsim 1000$ K, if its velocity is $\gtrsim 3$ km s^{-1}, which is a realistic velocity for an inner scale shock in our model.

7. ARE H_2O MASERS AN ADEQUATE PROBE OF SUPERSONIC TURBULENCE?

If the new conception of H_2O masers proposed here is correct, they may become an ideal tool for studying the properties of supersonic turbulence. In contrast to the large-scale ISM, supersonic turbulence probed by H_2O masers has only one source of energy, supplied at the largest scale: the interaction of the outflow from a young star with the surrounding gas. Furthermore, these flows are highly supervirial, so that gravitational effects are not important. Most probably, these flows are also super-Alfvénic. With the probable magnetic field strength $B \sim 10^{-3}$ G in the dense cores of molecular clouds and $B \sim 10^{-1}$ G in the H_2O maser clumps (Fiebig & Güsten 1989), and with the probable number densities of molecular hydrogen, $n \sim 10^6$ and 10^{10} cm^{-3}, respectively, the Alfvénic velocity is $v_A = B/(4\pi\rho)^{1/2} \approx B/(4\pi m_{H_2} n)^{1/2} \approx 2$ km s^{-1} in both cases. This is much less than the outer scale velocity ($v_L \approx 20$ km s^{-1}). Thus, turbulent velocities at most of the scales should be greater than the Alfvénic velocity, which means that the magnetic field does not constrain turbulent pulsations.

Masers are more effective than traditional ISM probes of turbulence, such as thermal or fluorescent spectral lines, from the observational standpoint. Maser lines are bright and narrow, which allows the spatial and kinematic structure of the associated flow to be measured with high precision. Because masing condensations are so small ($\lesssim 1$ mas), every spectral feature detected by the interferometer gives a direct measure of line-of-sight velocity at a given *point* in the flow, projected onto the sky. Indeed, the requirement of the velocity coherence along the line of sight (to produce lines with the observed widths $\lesssim 1$ km s^{-1}), together with the observed line-of-sight velocity gradients in the transverse direction of ~ 1 km s^{-1} AU^{-1}, and under the assumption that velocity gradients in the region are more or less isotropic, limits the probable length of a maser hot spot along the line of sight to $\lesssim 10$ AU. This is much less than the size of the whole active region ($\sim$10,000 AU) and allows us to consider the H_2O masers as pointlike probes of the velocity field, virtually as effective as the direct probes used to study terrestrial turbulent flows.

Doubts can arise on whether H_2O masers are an adequate probe of the geometry of the turbulence dissipation. For example, as a result of possible directivity of their radiation, some masing blobs may be unobserved. Can this distort the statistics we study? Obviously, the nonobservability of a fraction of places where turbulence dissipates results in underestimation of the space filling factor of dissipation. However, this will not affect the deduced fractal dimension of the set on which dissipation takes place, if all the "eddies," down to the smallest ones, contain *some* amount of observable masers. This follows from equation (4): reduction of σ by any factor (due to nonobservability of a fraction of the masers) will not change the value of the logarithmic derivative and thus the value of d.

If the directivity of the maser radiation is very high, it can affect observability of the smallest eddies, containing relatively small numbers of elementary masers. By an unlucky chance, all the masers within such an eddy could be turned away from the observer. The larger eddies, containing more elementary masers, should still be observable, although their contours will be delineated by reduced numbers of maser spots. A lack of observability of the smaller eddies will result in a decrease of β with the decreasing scale (see eq. [10]) and in a corresponding change of the slope of the plots in Figures 2–4. Using equations (8), (4), and (6), it is easy to convince oneself that this would steepen the slope of the plot toward the smallest scales in Figures 2 and 4 and flatten it toward the smallest scales in Figure 3. These effects are either unseen or quite small in these figures. We believe, therefore, that the majority of the scales, covering almost 4 orders of magnitude, are well represented by the H_2O masers and that d is determined adequately, regardless of possible omission of a fraction of the maser probes caused by radiation directivity.

8. CONCLUSIONS

Our conclusions are as follows:

1. VLBI maps of five H_2O maser sources in regions of star formation reveal fractal spatial distribution of the masing hot spots, a power-law dependence of two-point velocity

increments on spatial scale, and the non-Gaussian statistics of velocity increments (a strong excess of large deviations from the mean value). All these properties are known as typical of turbulence.

2. If the H_2O masers indeed trace turbulence, our quantitative analysis shows that this highly supersonic turbulence is characterized by a much lower fractal dimension ($d \lesssim 1$), and thus much stronger intermittency, than incompressible turbulence. Strong intermittency at virtually all the spatial scales is also confirmed by the excess of large velocity increments at all scales.

3. Unexpectedly, the power indices of the low-order velocity structure functions for the putative supersonic turbulence are found to be close to the classic Kolmogorov values for high Reynolds number incompressible turbulence. This is incompatible with the strong intermittency (low fractal dimension) in traditional approaches to turbulence but may find its explanation in the framework of the new approach put forward by BC97.

4. Supersonic turbulence with a high Mach number at its greatest scale may possess an inner scale, at which the bulk of its energy is dissipated in low Mach number stochastic shocks. The predicted value of the inner scale is close, by the order of magnitude, to the observed sizes of the H_2O hot spots. We hypothesize that the H_2O masers are generated in the random shocks at the inner scale of highly supersonic turbulence produced in the ambient gas by the intensive outflow from a newly born star.

S. G. and B. H. acknowledge with gratitude support of their participation in this study by the NSF (Research Experiences for Undergraduates) grant AST 93-0039 and by the Nantucket Maria Mitchell Association.

REFERENCES

Alcolea, J., Menten, K. M., Moran, J. M., & Reid, M. J. 1992, in Astrophysical Masers, ed. A. W. Clegg & G. E. Nedoluha (Heidelberg: Springer), 225
Anderson, N., & Genzel, R. 1993, in Astrophysical Masers, ed. A. W. Clegg & G. E. Nedoluha (Berlin: Springer), 97
Barenblatt, G. I., & Chorin, A. 1997, Commun. Pure Appl. Math., 50, 381 (BC97)
Clegg, A., & Nedoluha, G. (ed.) 1993, Astrophysical Masers (Berlin: Springer)
Crownover, R. M. 1995, Introduction to Fractals and Chaos (Boston: Johns and Bartlett Publishers)
Dickman, R. L. 1985, in Protostars and Planets II, ed. D. C. Black & M. S. Matthews (Tucson: Univ. Arizona Press), 150
Dutton, J. A., & Deaven, D. G. 1969, Radio Sci., 4, 1341
Elitzur, M. 1992, Astronomical Masers (Dordrecht: Kluwer)
Elitzur, M., Hollenbach, D., & McKee, C. 1989, ApJ, 346, 983
Elmegreen, B. G. 1993, in Protostars and Planets III, ed. E. H. Levy & J. I. Lunine (Tucson: Univ. Arizona Press), 97
Falconer, K. J. 1990, Fractal Geometry, Mathematical Foundations and Applications (Chichester: Wiley)
Falgarone, E., Lis, D. C., Phillips, T. G., Pouquet, A., Porter, D. H., & Woodward, P. R. 1994, ApJ, 436, 728
Falgarone, E., & Phillips, T. G. 1990, ApJ, 359, 344
Falgarone, E., Phillips, T. G., & Walker, C. K. 1991, ApJ, 378, 186
Feder, J. 1988, Fractals (New York and London: Plenum Press)
Fiebig, D., & Güsten, R. 1989, A&A, 214, 333
Fleck, R. C., Jr. 1981, ApJ, 246, L151
Franco, J., & Carraminana, A. (ed.) 1999, Interstellar Turbulence (Cambridge: Cambridge Univ. Press)
Frisch, U. 1995, Turbulence (Cambridge: Cambridge Univ. Press)
Frisch, U., Sulem, P. L., & Nelkin, M. 1978, J. Fluid Mech., 87, 719
Genzel, R., et al. 1981, ApJ, 247, 1039
Gezari, S. 1997, BAAS, 29, 1243
Gezari, S., Reid, M. J., & Strelnitski, V. 1998, BAAS, 30, 1356
Gouyet, J.-F. 1996, Physics and Fractal Structures (Berlin: Springer)
Gwinn, C. 1994, ApJ, 429, 241
Gwinn, C. R., Moran, J. M., & Reid, M. J. 1992, ApJ, 393, 149
Holder, B., & Strelnitski, V. 1997, BAAS, 29, 1404
Hollenbach, D. J., McKee, C. F., & Chernoff, D. 1987, in Star Forming Regions, ed. M. Peimbert & J. Jugaku (Dordrecht: Reidel), 334
Kaufman, M. J., & Neufeld, D. A. 1996, ApJ, 456, 250
Kolmogorov, A. N. 1941a, Dokl. Akad. Nauk SSSR, 30, 9
Kolmogorov, A. N. 1941b, Dokl. Akad. Nauk SSSR, 31, 99
———. 1941c, Dokl. Akad. Nauk SSSR, 31, 538
———. 1962, J. Fluid Mech., 12, 82
Kylafis, N., & Norman, C. 1986, ApJ, 300, L73
———. 1987, ApJ, 323, 346
Larson, R. B. 1995, MNRAS, 272, 213
Mandelbrot, B. B. 1967, Science, 156, 636
———. 1982, The Fractal Geometry of Nature (New York: Freeman)
Masson, C. R., & Chernin, L. M. 1993, ApJ, 414, 230
Melnick, G. J., Menten, K. M., Phillips, T. G., & Hunter, T. 1993, ApJ, 416, L37
Migenes, V., & Reid, M. (ed.) 2002, IAU Symp. 206, Cosmic Masers: From Protostars to Black Holes (Dordrecht: Kluwer)
Obukhov, A. M. 1941, Dokl. Akad. Nauk SSSR, 32, 22
Reid, M. J. 1993, ARA&A, 31, 345
Reid, M. J., Hashick, A. D., Burke, B. F., Moran, J. M., Johnston, K. J., & Swenson, G. W., Jr. 1980, ApJ, 239, 89
Reid, M. J., Schneps, M. H., Moran, J. M., Gwinn, C. R., Genzel, R., Downes, D., & Rönnäng, B. 1988, ApJ, 330, 809
Richardson, L. F. 1922, Weather Prediction by Numerical Processes (Cambridge: Cambridge Univ. Press)
Scalo, J. M. 1987, in Interstellar Processes, ed. D. J. Hollenbach & H. A. Thronson, Jr. (Dordrecht: Reidel), 349
Schneps, M. H., et al. 1981, ApJ, 249, 124
Sellwood, J. A., & Balbus, S. A. 1999, ApJ, 511, 660
Shmeld, I. K., Strelnitski, V. S., & Muzylev, V. V. 1976, AZh, 53, 728
Spitzer, L. 1978, Physical Processes in the Interstellar Medium (New York: Wiley)
Strelnitski, V. S. 1984, MNRAS, 207, 339
Strelnitski, V. S., Alexander, J., Moran, J. M., & Reid, M. J. 1998, in ASP Conf. Ser. 144, Radio Emission from Galactic and Extragalactic Compact Sources, IAU Colloq. 164, ed. J. A. Zensus, G. B. Taylor, & J. M. Wrobel (San Francisco: ASP), 369
Strelnitski, V. S., & Sunyaev, R. A. 1973, Soviet Astron., 16, 579
Tarter, J., & Welch, W. J. 1986, ApJ, 305, 467
van Atta, C. W., & Park, J. 1972, in Statistical Models and Turbulence, ed. M. Rosenblatt & C. W. van Atta (Berlin: Springer), 402–426
von Weizsäcker, C. F. 1951, ApJ, 114, 165
Walker, R. C. 1984, ApJ, 280, 618
Walker, R. C., Matsakis, D. N., & Garcia-Barreto, J. A. 1982, ApJ, 255, 128